Structure and Sodium Channel Activity of an Excitatory I_1-Superfamily Conotoxin[†,‡]

Olga Buczek,[§,∥] Daxiu Wei,[§,⊥] Jeffrey J. Babon,[⊥] Xiaodong Yang,[⊥] Brian Fiedler,[∥] Ping Chen,[∥] Doju Yoshikami,[∥] Baldomero M. Olivera,[∥] Grzegorz Bulaj,[#] and Raymond S. Norton*[,⊥]

Department of Biology, University of Utah, Salt Lake City, Utah 84112, The Walter and Eliza Hall Institute of Medical Research, 1G Royal Parade, Parkville 3050, Australia, and Department of Medicinal Chemistry, University of Utah, Salt Lake City, Utah 84108

Received April 27, 2007; Revised Manuscript Received July 3, 2007

ABSTRACT: Conotoxin ι-RXIA, from the fish-hunting species *Conus radiatus*, is a member of the recently characterized I_1-superfamily, which contains eight cysteine residues arranged in a -C-C-CC-CC-C-C- pattern. ι-RXIA (formerly designated r11a) is one of three characterized I_1 peptides in which the third last residue is posttranslationally isomerized to the D configuration. Naturally occurring ι-RXIA with D-Phe44 is significantly more active as an excitotoxin than the L-Phe analogue both in vitro and in vivo. We have determined the solution structures of both forms by NMR spectroscopy, the first for an I_1-superfamily member. The disulfide connectivities were determined from structure calculations and confirmed chemically as 5−19, 12−22, 18−27, and 21−38, suggesting that ι-RXIA has an ICK structural motif with one additional disulfide (21−38). Indeed, apart from the first few residues, the structure is well defined up to around residue 35 and does adopt an ICK structure. The C-terminal region, including Phe44, is disordered. Comparison of the D-Phe44 and L-Phe44 forms indicates that the switch from one enantiomer to the other has very little effect on the structure, even though it is clearly important for receptor interaction based on activity data. Finally, we identify the target of ι-RXIA as a voltage-gated sodium channel; ι-RXIA is an agonist, shifting the voltage dependence of activation of mouse $Na_V1.6$ expressed in *Xenopus* oocytes to more hyperpolarized potentials. Thus, there is a convergence of structure and function in ι-RXIA, as its disulfide pairing and structure resemble those of funnel web spider toxins that also target sodium channels.

Through adaptive evolution, marine cone snails of the genus *Conus* have generated more than 70000 different venom peptides (conopeptides) (*1*−*3*). These highly diverse peptides can be organized into several structural classes, with peptides in the same structural class generally belonging to the same gene superfamily. The peptides in a given superfamily share a highly conserved precursor signal sequence and a disulfide scaffold with a characteristic number, pattern, and pairing of cysteine residues in the mature toxin (*1*−*3*). Thus, despite hypermutation of amino acids between half-cystines, the disulfide framework remains conserved within a superfamily. In addition to the accelerated evolution of conopeptide sequences, further molecular diversity is introduced through posttranslational modifications. The occurrence of diverse modifications in *Conus* peptides is now well established (*4*), but the functional consequences of most posttranslational modifications remain unknown, and mechanistic insights require detailed structure/function analyses, which have not been performed in most cases.

Recently, we described the I-superfamily of *Conus* peptides, defined by framework 11, with eight cysteine residues arranged in two pairs of adjacent Cys flanked by nonadjacent Cys residues (-C-C-CC-CC-C-C-) (*5*−*7*). A preliminary analysis of *Conus* cDNA clones reveals that framework 11 peptides are found broadly across the genus, and an extreme diversity of sequences is observed (*7*, *8*). For example, 17 different cDNA clones were identified in the venom of *Conus radiatus* alone. These varied toxins, though sharing the same cysteine arrangement, can be divided into two distinct genetic groups, designated the I_1- and I_2-superfamilies (*7*). Members of the I_1-class have been isolated from the fish-hunting species *Conus radiatus* (*5*) and members of the I_2-class from worm-hunting species such as *Conus betulinus* (*9*) and *Conus virgo* (*10*). I_1-superfamily conotoxins are excitatory (*5*−*7*), and, as we show in this report, the most extensively studied of these, ι-RXIA[1] (formerly known as r11a) (*11*), targets the $Na_V1.6$ subtype of voltage-gated sodium channels (VGSC) but had no effect on KCNQ2/3 and several members of the K_V1 family of potassium channels tested. In contrast, two I_2-superfamily peptides have been shown to target specific

[†] This work was supported in part by NIH Grant GM 48677 (to B.M.O.) from the National Institute of General Medical Sciences. R.S.N. acknowledges support from the Australian National Health and Medical Research Council.

[‡] Chemical shift assignments for ι-RXIA[L-Phe44] and ι-RXIA have been deposited in the BioMagResBank with accession numbers 15174 and 15175, respectively. The families of structures of ι-RXIA[L-Phe44] and ι-RXIA have been deposited in the Protein Data Bank with accession numbers 2P4L and 2JRY, respectively.

* To whom correspondence should be addressed. E-mail: ray.norton@wehi.edu.au. Phone: +61 3 9345 2306. Fax: +61 3 9345 2686.

[§] These authors contributed equally to this work.

[∥] Department of Biology, University of Utah.

[⊥] The Walter and Eliza Hall Institute of Medical Research.

[#] Department of Medicinal Chemistry, University of Utah.

[1] Abbreviations: IAA, iodoacetic acid; I_{Na}, sodium current; ι-RXIA, iota-conotoxin RXIA (previously designated r11a); K_V, voltage-gated potassium channel(s); Na_V or VGSC, voltage-gated sodium channel; NEM, *N*-ethylmaleimide; NMR, nuclear magnetic resonance; NOE, nuclear Overhauser effect; TCEP, tris(2-carboxyethyl)phosphine hydrochloride; TFA, trifluoroacetic acid.

10.1021/bi700797f CCC: $37.00
Published on Web 08/14/2007

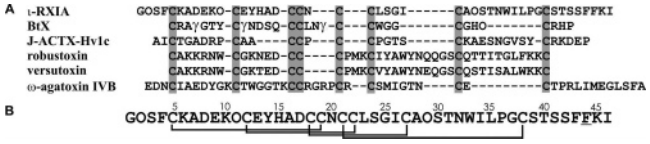

FIGURE 1: Amino acid sequence and disulfide connectivities. (A) Comparison of various toxin sequences containing four disulfide bridges; the first three have a framework 11 pattern of half-cystine spacings (-C-C-CC-CC-C-C-). SwissProt accession numbers are as follows: ι-RXIA, Q7Z094; BtX, Q9U3Z3; J-atracotoxin Hv1c, P82228; robustoxin, P01478; versutoxin, P13494; ω-agatoxin IVB, P37045. In the I_2-superfamily conotoxin BtX, all three Glu residues in the mature toxin sequence are γ-carboxy-Glu (*9*). (B) Amino acid sequence of ι-RXIA showing disulfide connectivities determined in this work by NMR and chemical mapping. The underlined residue, Phe44, has a D configuration.

K^+ channels, namely, the Ca^{2+}- and voltage-sensitive BK channels (*9*), and the $K_V1.1$ and $K_V1.3$ channel subtypes of the Shaker subfamily (*10*).

Although framework 11 defines the I-superfamily of *Conus* peptides, peptides with the same pattern of half-cystines have also been found in the venoms of Australian funnel web spiders (*12*). Figure 1A compares the sequences of three framework 11 peptides, two from *Conus* and one from a spider. Three other spider toxins with four disulfide bridges, although not in a framework 11 pattern, are also shown as they are discussed below. These toxins target a range of ion channels, including Na^+, Ca^{2+}, and possibly K^+ channels (*12*−*16*).

For ι-RXIA, a clear demonstration of the functional importance of one posttranslationally modified amino acid was reported recently (*6*). This 46-residue conotoxin contains a D-Phe residue in position 44, three residues from the C-terminus. The naturally occurring peptide and its synthetic counterpart (with D-Phe44) were equipotent in eliciting repetitive action potentials in axons, whereas the L-Phe44-containing analogue was inactive in this assay and 10−20-fold less active than ι-RXIA in an in vivo assay (*6*). In order to explore the relationship between structure and activity of ι-RXIA, we have determined the solution structure of the L-Phe44-containing peptide and compared it with the D-Phe44 form. The structure was similar to those of funnel web spider toxins that target Na^+ channels. We then showed that ι-RXIA was an agonist of the $Na_V1.6$ sodium channel, shifting its voltage dependence of activation to more hyperpolarized potentials, but had no effect on several members of the K_V1 family of potassium channels tested.

EXPERIMENTAL PROCEDURES

Peptide Synthesis and Oxidative Folding. Peptides ι-RXIA and ι-RXIA[L-Phe44] were synthesized on solid supports by an automated peptide synthesizer using N-Fmoc [*N*-(9-fluorenyl)methoxycarbonyl]-protected amino acids, 2-(1*H*-benzotriazol-1-yl)-1,1,3,3-tetramethyluronium hexafluorophosphate (HBTU), and diisopropylethylamine (DIEA), courtesy of Dr. Robert Schackmann of the DNA/Peptide Facility, University of Utah. All cysteine residues were trityl-protected; the coupling time was 1 h. Peptide cleavage/deprotection was accomplished with reagent K [82.5% TFA (trifluoroacetic acid):5% phenol:5% H_2O:5% thioanisole:2.5% 1,2-ethanedithiol] for 2 h at room temperature. Soluble crude peptides were precipitated with cold methyl *tert*-butyl ether (MTBE) and centrifuged. The pellet was washed with methyl *tert*-butyl ether, centrifuged again, then dissolved in 25% acetonitrile in 0.1% TFA, and lyophilized. The linear peptides were purified on a Vydac C_{18} semipreparative HPLC column with a gradient of 30−60% solvent B (0.1% TFA in 90% acetonitrile; solvent A was 0.1% TFA in water) over 30 min at a flow rate of 3 mL/min.

Oxidative folding of the peptides was carried out in a solution of 0.1 M Tris-HCl, pH 8.7, containing 1 mM EDTA, 1 mM oxidized glutathione, and 1 mM reduced glutathione at room temperature for 3 h. The reaction was initiated by adding the linear synthetic peptide to a final concentration of 20 μM and then quenched by adding formic acid to a final concentration of 8%. The oxidized peptide was purified on a Vydac C_{18} semipreparative HPLC column with a gradient of 15−60% solvent B over 40 min at a flow rate of 3 mL/min.

Disulfide Mapping of ι-RXIA. The disulfide-bonding framework of ι-RXIA was determined by the partial reduction (*17*) and stepwise alkylation method. Ten nanomoles of oxidized peptide was dissolved in 100 μL of 20% acetonitrile in water and partially reduced by addition of 120 μL of 20 mM TCEP in 0.2 M sodium citrate, pH 3.0, and incubation for 5 min at room temperature. The reaction was stopped by immediate injection on a Vydac C_{18} analytical HPLC column equilibrated at 45 °C, and the partially reduced intermediates were eluted with a shallow gradient of 32−38% solvent B over 1 h at a flow rate of 1 mL/min. Individual partially reduced species were collected manually and stored at −20 °C for no longer than 2 h before the first alkylation. Typically, the fractions from two independent runs were pooled and contained about 0.5−1 nmol of peptide in 2 mL of solvent.

For alkylation with NEM (*N*-ethylmaleimide) an equivalent volume (2 mL) of 60 mM NEM in 0.2 M sodium citrate, pH 3.0, was added directly to the fraction containing partially reduced peptide. After incubation for 1 h at room temperature, the mixture was applied to a Vydac C_{18} analytical HPLC column, equilibrated at 45 °C, and eluted with 30% solvent B for 15 min followed by a gradient of 30−55% solvent B for 25 min and then by a gradient of 55−100% solvent B for 5 min at a flow rate of 1 mL/min. Collected fractions were dried and stored at −20 °C for no longer than overnight. The first alkylation yielded between 0.25 and 1 nmol of a single species of NEM-labeled peptide.

For the complete reduction and alkylation with IAA (iodoacetic acid), the NEM-labeled peptide (∼1 nmol) was dissolved in 40 μL of 50% acetonitrile in 0.1% TFA and reduced by addition of 10 μL of reducing buffer (0.5 M Tris−acetate, pH 8.0, containing 5 mM EDTA and 100 mM dithiothreitol) and incubation at 65 °C for 30 min. The peptide was then alkylated with 40 μL of 0.5 M IAA in 0.5 M Tris−acetate, pH 8.0, containing 5 mM EDTA in the dark at room temperature for 30 min. The reaction mixture was applied to a Vydac C_{18} analytical HPLC column, equilibrated at 45 °C, and eluted as described above for the first-step alkylation.

The completed partial reduction and stepwise alkylation yielded between 0.1 and 0.3 nmol of a given species of NEM- and IAA-double-labeled product, starting from 80 to 100 nmol of oxidized peptide. The doubly alkylated variants

of ι-RXIA were sequenced by standard automated Edman degradation performed with an Applied Biosystem Model 492 sequenator, courtesy of Dr. Robert Schackmann of the DNA/Peptide Synthesis Facility, University of Utah.

Mass Spectrometry. Matrix-assisted laser desorption ionization (MALDI) mass spectra of the native and synthetic peptides were obtained using a Bruker REFLEX time-of-flight mass spectrometer (Bruker Daltonics) fitted with gridless reflectron, an N_2 laser, and a 100 MHz digitizer at the Salk Institute for Biological Studies (La Jolla, CA).

Mass spectrometry of partially reduced forms of ι-RXIA was performed with a Sciex API-III electrospray ionization (ESI) quadruple mass spectrometer, courtesy of Dr. Chad Nelson of the Mass Spectrometry and Proteomics Core Facility, University of Utah. Molecular masses of all variants were within 1.0 amu of calculated values.

NMR Spectroscopy. Samples were prepared for NMR by dissolving lyophilized peptide in 95% H_2O/5% ^2H_2O to a final peptide concentration of 1.1 mM for ι-RXIA[L-Phe44] and 0.8 mM for ι-RXIA. At 5 and 25 °C, a series of one-dimensional spectra was collected at pH 2.8, 5.9, and 6.9, respectively, for both peptides. Two-dimensional homonuclear TOCSY with a spin-lock time of 70 ms, DQF-COSY, and NOESY spectra were recorded at pH 5.9 on Bruker DRX-600 and Avance 800 spectrometers. NOESY spectra were recorded at mixing times of 50, 100, 250, and 300 ms. A 250 ms NOESY spectrum was used for resonance assignments and NOE intensity measurements. To monitor backbone amide exchange, a series of 1D spectra was recorded at various time intervals for the sample in 100% ^2H_2O at 278 K on the 600 MHz spectrometer. For ι-RXIA, the translational diffusion coefficient was measured at 5 °C using a PFG longitudinal eddy-current delay pulse sequence (*18*, *19*), as implemented by Yao et al. (*20*). Spectra were referenced to an impurity peak at 0.15 ppm which has been referenced previously against the internal standard dioxane (3.75 ppm) and does not vary with solution conditions over the pH and temperature range used in this study. Spectra were processed using TopSpin, version 1.3, and analyzed using XEASY, version 1.3.13 (*21*). $^1H-^{13}C$ HSQC spectra for the assignment of ^{13}C chemical shifts and a $^1H-^{15}N$ HSQC spectrum for the assignment of ^{15}N chemical shifts (*22*, *23*) were collected at 25 °C on a Bruker Avance 500 spectrometer equipped with a cryoprobe. ^{15}N and ^{13}C chemical shifts are presented in Tables S1 and S2 in Supporting Information.

Structure Calculations. Distance constraints were taken from the volumes of NOESY cross-peaks at 25 °C, pH 5.9, and 800 MHz. NOE buildup rates were monitored for a number of cross-peaks at 25 °C, pH 5.9, and 600 MHz, as shown in Figure S1 in Supporting Information. $^3J_{HNH\alpha}$ values were measured from a DQF-COSY spectrum and converted to φ dihedral restraints as follows: $^3J_{HNH\alpha} > 8$ Hz, $\varphi = -120 \pm 40°$; $^3J_{HNH\alpha} < 6$ Hz, $\varphi = -60 \pm 30°$. For residues with $6 < {}^3J_{HNH\alpha} < 8$ Hz, if NOE data showed they did not have positive φ angles, restraints with $\varphi = -90 \pm 90°$ were applied in the structure calculation. χ^1 angles for residues 5, 6, 8, 10, 12, 14, 17, 18, 21, and 27 were determined by analyzing NOESY spectra with a short mixing time of 50 ms. Intensities of NOE cross-peaks measured in XEASY were calibrated using the CALIBA macro from the program CYANA (*24*). Initial structures were calculated using torsion angle dynamics and simulated annealing protocols in CYANA, and structures were optimized for a low target function. These structures were used to identify hydrogen bond partners for backbone amide protons that were found to be in slow or intermediate exchange with solvent; where such an amide formed a bond with the same partner in ≥80% of the CYANA structures, this hydrogen bond was included as a restraint in the final round of structure calculations. For each hydrogen bond constraint, upper limits of 2.4 and 3.3 Å were used for the distances from proton to acceptor and donor nitrogen atom to acceptor, respectively. The final constraint set was then used to calculate a new family of 200 structures using XPLOR-NIH (*25*). The 50 lowest energy structures were selected for energy minimization in a box of water. A final family of 20 lowest energy structures was chosen for analysis using PROCHECK-NMR (*26*) and MOLMOL (*27*). The 30 lowest energy structures before water refinement had no experimental distance violations >0.3 Å or dihedral angle violations >5°. For the final 20 structures after water refinement, no distance violations >0.3 Å or dihedral angle violations >5° were present. Structural figures were prepared using MOLMOL (*27*), PyMol (*28*), and GRASP (*29*).

Electrophysiology. The clone for the mouse $Na_V1.6$ channel subtype was kindly provided by Alan Goldin, and cRNA was prepared from it by Layla Azam. Clones for human KCNQ2/3 and $K_V1.2-1.6$ were purchased from PROTINAC GmbH, Hamburg, Germany, and corresponding cRNAs were produced using the mMessage mMachine RNA trancription kit from Ambion (Austin, TX). Each oocyte was injected with 1.5 ng of $Na_V1.6$, 2.5 ng of KCNQ2 plus 2.5 ng KCNQ3, or 5 ng ($K_V1.2$, -1.3, -1.4, -1.5 or -1.6) of cRNA in 50 nL of distilled water and incubated at 16 °C in ND96 (composition in millimolar: 96 NaCl, 2 KCl, 1.8 $CaCl_2$, 1 $MgCl_2$, 5 HEPES, pH ∼7.3) supplemented with Pen/Strep, Septra, and Amikacin for 2−6 days. The recording chamber consisted of a cylindrical well (4 mm diameter, total volume ∼30 μL) in a wafer made of Sylgard (Dow Corning, Midland, MI). Oocytes were two-electrode voltage clamped with a Warner OC-725C amplifier (Warner Instruments, Hamden, CT) using glass microelectrodes filled with 3 M KCl (0.1−0.5 MΩ resistance). The chamber was perfused with ND96 for $Na_V1.6$ or KCM 4.1.1 (96 mM NaCl, 4 mM KCl, 1 mM $CaCl_2$, 1 mM $MgCl_2$, 5 mM HEPES) for KCNQ2/3 or frog Ringer's (115 mM NaCl, 2.5 mM KCl, 1.8 mM $CaCl_2$, 10 mM HEPES, pH 7.4) for K_V1 channels. Both solutions also contained 0.1 mg/mL bovine serum albumin. For $Na_V1.6$, the membrane potential was held at −100 mV, and VGSCs were activated by 60 ms depolarizing steps applied every 20 s; the protocol for inactivation measurements was essentially the same except a 30 ms test pulse to −10 mV was applied immediately after a 500 ms conditioning pulse of varying amplitude. For KCNQ2/3, the membrane potential was held at −80 mV, and channels were activated by a 2 s step to 0 mV applied every 10 s. After each pulse, deactivating ("tail") currents were recorded at a potential of −60 mV. For K_V1 channels, the membrane potential was held at −90 mV, and channels were activated by a 150 ms step to +20 mV applied every 60 s. Current signals were low-pass filtered at 2 kHz ($Na_V1.6$) or 1 kHz (potassium channels), digitized at a sampling frequency of 10 kHz, and leak-subtracted by a P/6 protocol using in-house

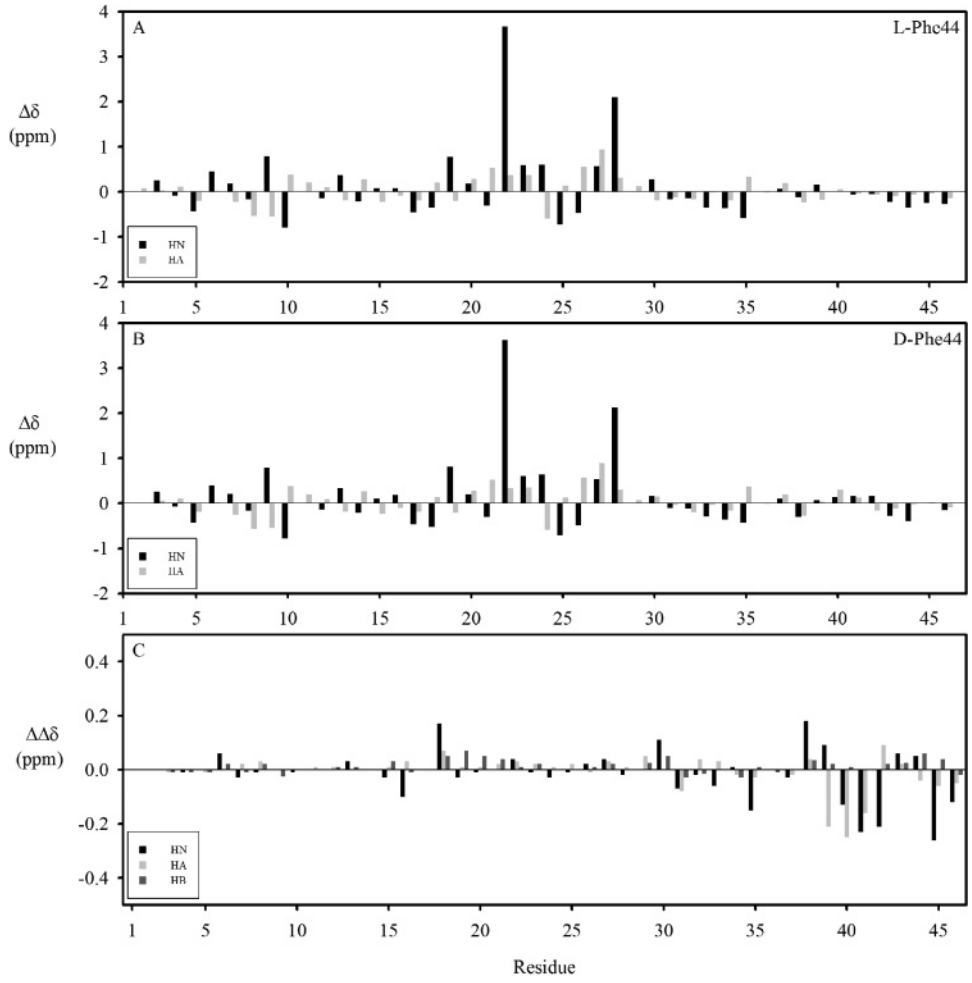

FIGURE 2: Deviations of ι-RXIA[L-Phe44] (A) and ι-RXIA (B) chemical shifts from random coil values at 298 K. The NH and $C^{\alpha}H$ random coil chemical shifts are from ref *31*. (C) Chemical shift differences of HN, $C^{\alpha}H$, and $C^{\beta}H$ resonances between ι-RXIA[L-Phe44] and ι-RXIA.

software written in LabVIEW (National Instruments, Austin, TX). Voltage dependencies of activation and inactivation data were curve-fit to the Bolzmann equation using Graphpad Prism (GraphPad Software, San Diego, CA). ι-RXIA was dissolved in ND96 (for $Na_V1.6$), KCM 4.1.1 (for KCNQ2/3), or Ringer's (for K_V1 channels) with 0.1 mg/mL bovine serum albumin and applied by halting the perfusion, injecting 3 μL of peptide solution (at ten times the final concentration) into the 30 μL bath with a pipettor, and manually stirring the bath for about 5 s by gently aspirating and expelling ~5 μL of bath fluid several times with the pipettor. Responses in the presence of peptide, as well as control responses, were acquired in static baths to conserve peptide. All experiments were conducted at room temperature (~22 °C).

RESULTS

Peptide Synthesis. Two variants of ι-RXIA, with L- or D-Phe44, were synthesized on a solid support using a standard Fmoc protocol. Peptides were folded in the presence of oxidized and reduced glutathione as described in Experimental Procedures. The HPLC profiles of the folding reactions for the L- or D-Phe44 forms of ι-RXIA were identical, and the yield of oxidation was about 80% in both cases. As shown previously by HPLC coelution experiments, the fully oxidized form of the peptide containing D-Phe44 was identical to the natural toxin isolated from the venom of *C. radiatus* (*6*). In this paper we refer to the D-Phe44 version of the peptide simply as ι-RXIA and the L-Phe44 version as ι-RXIA[L-Phe44]. Both synthetic variants of ι-RXIA were used to determine and compare the solution structures, while the cysteine bridging pattern was determined chemically for the biologically active, D-Phe44-containing variant.

NMR Spectroscopy. One-dimensional ^1H NMR spectra of ι-RXIA[L-Phe44] at pH 2.8, 5.9, and 6.9 indicated that the toxin was partially denatured at the lower pH but well structured at both pH 5.9 and pH 6.9 (Figure S2 in Supporting Information). One- and two-dimensional spectra recorded at 5 and 25 °C showed that only one conformation was present in aqueous solution. Although ι-RXIA contains one proline and three hydroxyproline residues, there was no evidence of *cis*−*trans* isomerization in either ι-RXIA or ι-RXIA[L-Phe44].

Sequence-specific chemical shift assignments for backbone and side-chain protons were made at 600 and 800 MHz by analyzing standard two-dimensional homonuclear NMR spectra. Assignments at 25 °C and pH 5.9 for ι-RXIA[L-Phe44] and ι-RXIA are tabulated in Tables S1 and S2 in Supporting Information and deposited in BioMagResBank (*30*) with accession numbers 15174 and 15175, respectively.

Figure 2 shows the deviations of the backbone NH and $C^{\alpha}H$ chemical shifts from random coil values (*31*) at 25 °C for ι-RXIA[L-Phe44] (Figure 2A) and ι-RXIA (Figure 2B). For ι-RXIA, the translational diffusion coefficient at 5 °C was $(1.17 \pm 0.04) \times 10^{-10}$ m^2 s^{-1}. This is lower than the corresponding value of $(1.38 \pm 0.03) \times 10^{-10}$ m^2 s^{-1} at 5 °C for Magi 5, a 29-residue spider toxin with a compact ICK motif structure (*32*), reflecting the larger mass of ι-RXIA and its more extended C-terminal tail (described below).

Structural Restraints. We determined the structures of ι-RXIA and ι-RXIA[L-Phe44], but the ι-RXIA[L-Phe44] structure is described first because a larger quantity was available, yielding better spectra. Analysis of a DQF-COSY spectrum showed that $^3J_{HN\alpha}$ coupling constants of Cys18, Asn20, Cys21, Leu23, Ser24, Ala28, Thr31, Asn32, and Trp33 were >8 Hz and there were none <6 Hz. Amide exchange experiments of ι-RXIA[L-Phe44] conducted at 5 °C and pH 5.9 indicated that the amide protons of Cys12, Asn20, Cys21, Leu23, Ile26, Cys27, and Ala28 were the slowest to exchange, those of Glu9, Cys19, Cys18, Tyr14, Gly25, and Lys10 had intermediate exchange residues, and the rest exchanged with solvent within minutes of dissolution of the polypeptide in ^2H_2O.

The disulfide bond pairings were determined by preliminary structure calculations in CYANA. First, a family of 20 structures was determined in CYANA based only on distance constraints. Distances were then measured between pairs of Cys S atoms and pairs of Cys $C^{\beta}H$ protons. As a result, it was obvious that Cys5 and Cys19 were much closer to one another than to other Cys residues, as were Cys21 and Cys38. To determine the other two disulfide bond pairings, structure calculations, including the above two disulfide connectivities, were repeated with six possible combinations among Cys12, Cys22, Cys18, and Cys27. It was found that the combination of Cys12−Cys22 and Cys18−Cys27 had the lowest energies and fewest NMR restraint violations compared with other possible combinations. This pattern suggests that ι-RXIA[L-Phe44] has an ICK motif structure (*33*−*35*) with one additional disulfide (Cys21−Cys38), as shown in Figure 1B.

Disulfide Mapping of ι-RXIA. The disulfide connectivities were confirmed by partial reduction of the peptide with TCEP followed by stepwise alkylation and microsequencing of the final product. Key features of the strategy were optimization of the reaction to yield the highest ratio of partially reduced disulfide species relative to fully reduced peptide and proper choice of alkylating agent. The rearrangement of disulfide bonds was avoided by performing the first alkylation with *N*-ethylmaleimide (NEM) at an acidic pH directly after HPLC separation of the partially reduced forms. The second labeling was done with iodoacetic acid (IAA), as NEM- and IAA-labeled cysteines are readily distinguishable during microsequencing.

Figure 3A shows the HPLC elution of partially reduced ι-RXIA. Four out of five major partially reduced forms were separated and analyzed by ESI mass spectrometry. Their molecular masses were determined to be 4976.5, 4978.1, 4978.2, and 4979.9 Da, corresponding to species containing three, two, two, and one remaining disulfide bond, respectively. We refer to these partially reduced intermediates as 3S-S, 2S-S1, 2S-S2, and 1S-S species. The first alkylation of each intermediate gave one main product, which was repurified by HPLC (Figure 3B). Each alkylated variant was then lyophilized and resuspended in the pH 8.0 buffer, and the remaining disulfides were reduced and the free cysteines labeled with IAA. The double-labeled species appeared as one major peak during purification with RP-HPLC (Figure 3C).

Four different alkylated variants of ι-RXIA (3S-S, 2S-S1, 2S-S2, and 1S-S) were sequenced to identify the labeling pattern of cysteine residues. Although the microsequencing data were clear, a few factors made the analysis challenging. First, ι-RXIA is a large, rather hydrophobic peptide, and after double alkylation and lyophilization it remained almost insoluble. Thus, the sequencing was performed directly after HPLC with 0.5−1 mL fractions containing about 300 pmol of the peptide loaded overnight. The other challenge was to identify the IAA labeling when Cys was in very close proximity to Ser as those two signals could not be separated. Furthermore, in the case of species with two remaining disulfides (2S-S1 and 2S-S2) the signal for the last cysteine residue (position 38 in the sequence) was too low to identify the labeling. Figure 3D shows the cysteine-labeling pattern resulting from microsequencing data and the surmised disulfide connectivity of ι-RXIA. This was in perfect agreement with the disulfide connectivities determined by NMR for ι-RXIA[L-Phe44], showing that both forms of this polypeptide fold in the same way.

Solution Structure of ι-RXIA[L-Phe44]. Parameters characterizing the final 20 structures in X-PLOR and structural statistics for ι-RXIA[L-Phe44] are summarized in Table 1, and stereoviews of the family of structures superimposed over the backbone heavy atoms are shown in Figure 4A. Numerous medium- and long-range NOEs ($i - j > 4$) were observed for residues 5−30 (Figure S3 in Supporting Information), implying that this region has a well-defined structure. By contrast, very few medium- or long-range NOEs were observed for the N- and C-terminal regions, indicating that both termini lacked a well-defined structure in solution.

The angular order parameters *S* for the φ, ψ, and χ^1 angles in the final family of 20 structures (Figure S3 in Supporting Information) show that the structured region of ι-RXIA[L-Phe44] encompasses residues 5−35. The RMSD over the backbone heavy atoms was 0.49 Å for Cys5−Ser30 and 1.64 Å for Cys5−Leu35. The closest to average structure is shown in Figure 4B,C. The structures of ι-RXIA[L-Phe44] have been deposited with the RCSB Protein Data Bank (*36*) with accession number 2P4L.

Of the four disulfide bridges (Cys5−Cys19, Cys12−Cys22, Cys18−Cys27, and Cys21−Cys38), the first three are located in the well-defined region of the structure. The separation of the half-cystines in this region, $-CX_6CX_5C-CX_2CX_4C-$, where X is any amino acid, fits the original consensus for an ICK motif structure, $-CX_{3-7}CX_{3-6}CX_{0-5}-CX_{1-4}CX_{4-13}C-$(*33*, *34*). Secondary structure analysis using PROCHECK (*26*) showed that ι-RXIA contained a small, two-stranded, antiparallel β-sheet (Cys21−Cys22 and Cys27−Ala28). The fourth disulfide, Cys21−Cys38, links the ICK motif to the C-terminal region. An examination of amide exchange data as well as the ensemble of structures suggested that hydrogen bonds exist between the following pairs of residues: Cys27 and Glu9, Cys21 and Ala28, Leu23 and Ile26, Cys19 and Lys6, Cys12 and Cys22, and Lys10 and

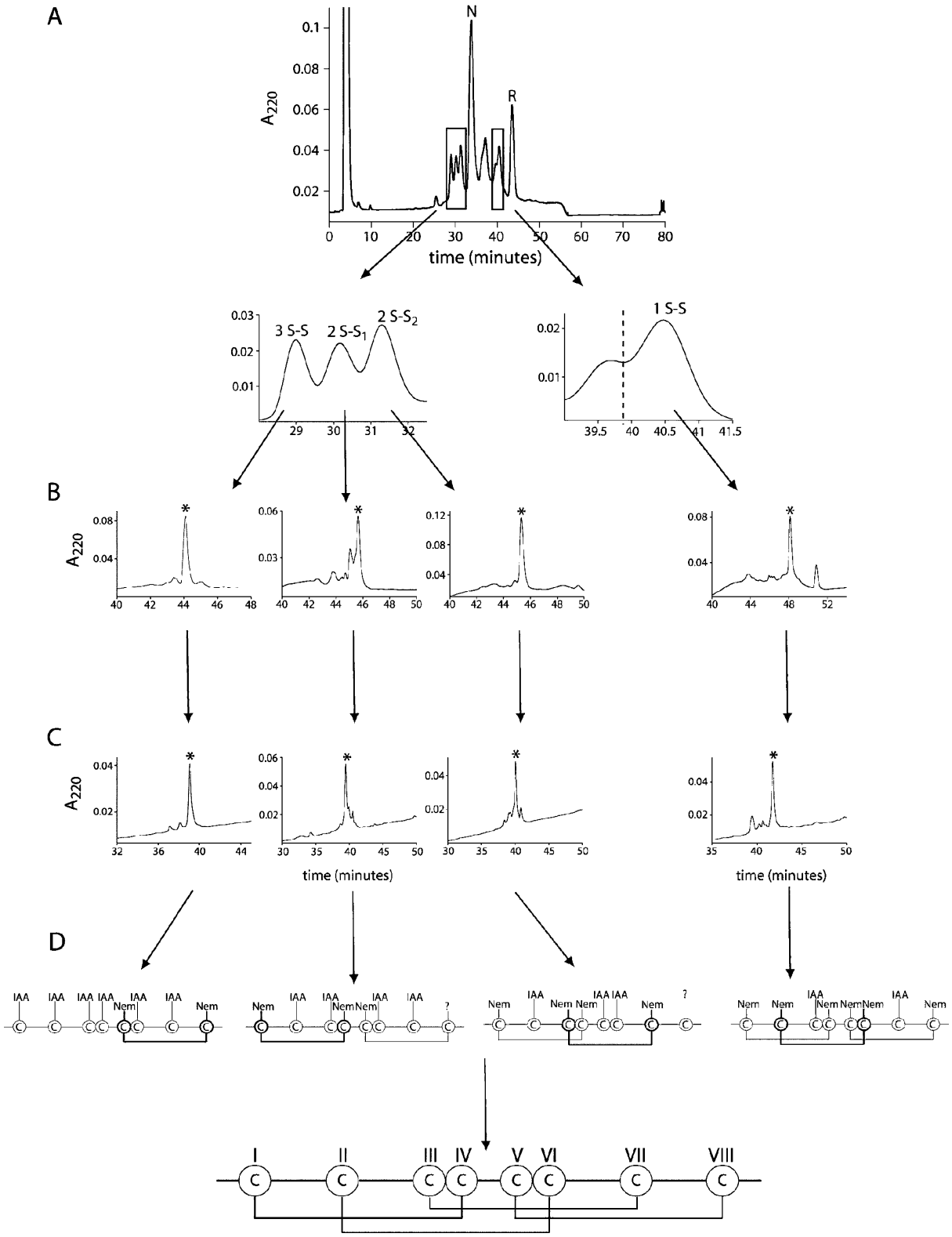

FIGURE 3: Disulfide mapping of ι-RXIA. (A) HPLC trace for TCEP partial reduction of ι-RXIA. The reaction was carried out with 20 mM TCEP in 0.2 M sodium citrate, pH 3.0, for 5 min at room temperature. N and R denote the native and reduced form, respectively. Four major partially reduced forms, which correspond to the species containing three (3S-S), two (2S-S_1 and 2S-S_2), and one (1S-S) remaining disulfide bond, were separated. (B) HPLC traces for purification of NEM-alkylated variants. The reaction was performed with 60 mM NEM in 0.2 M sodium citrate, pH 3.0, for 1 h at room temperature directly after HPLC separation of partially reduced forms. (C) HPLC purification of double-labeled forms. The NEM-alkylated variants were completely reduced and then alkylated with 0.2 M IAA in 0.2 M Tris−acetate and 0.2 mM EDTA, pH 8.0, for 30 min at room temperature. Each proper product is marked with an asterisk. (D) Schematic representation of a labeling pattern of cysteine residues resulting from the microsequencing data and disulfide connectivity of ι-RXIA.

Asp8. These are all part of, or adjacent to, the two-stranded β-sheet that forms the core of the structure. An examination of backbone φ and ψ angles as well as hydrogen bonds in the final family of structures indicated that residues 8−10 form a γ-turn, with Glu9 having a positive φ angle. An interesting feature of the structured region of ι-RXIA[L-

Table 1: Experimental Constraints and Structural Statistics for ι-RXIA[L-Phe44] and ι-RXIA

	ι-RXIA[L-Phe44]	ι-RXIA
no. of distance restraints		
total	482	448
intraresidue ($i = j$)	223	198
sequential ($\|i - j\| = 1$)	156	132
medium range ($1 < \|i - j\| < 5$)	38	22
long range ($\|i - j\| > 4$)	65	96
hydrogen bond restraints	9	7
no. of dihedral restraints	49	39
RMSD from exptl data		
NOEs (Å)	0.021 ± 0.004	0.027 ± 0.004
dihedrals (deg)	0.560 ± 0.2	0.299 ± 0.2
deviations from ideal[a]		
angles (deg)	0.675 ± 0.03	0.707 ± 0.04
bonds (Å)	0.0046 ± 0.0006	0.0048 ± 0.0006
impropers (deg)	0.486 ± 0.03	0.486 ± 0.03
RMSD[b] for residues 5−30		
all heavy atoms	1.07 ± 0.17	1.17 ± 0.21
backbone heavy atoms (N, C^α, C)	0.49 ± 0.15	0.56 ± 0.13
RMSD[b] for residues 5−35		
all heavy atoms	2.28 ± 1.10	2.17 ± 0.43
backbone heavy atoms (N, C^α, C)	1.64 ± 1.04	1.39 ± 0.38
Ramachandran plot[b]		
most favored (%)	50.0	52.4
allowed (%)	42.3	38.5
additionally allowed (%)	4.4	5.9
disallowed (%)	3.3	3.2

[a] The values for the bonds, angles, and impropers show the deviations from ideal values based on perfect stereochemistry. [b] As determined by the program PROCHECK-NMR for all residues. The high percentage of residues in the disallowed residue of the Ramachandran plot reflects the positive φ angle for Glu9. All violations, energies, and RMS differences are given as the mean ± standard deviation.

Phe44] is the abundance of charged side chains (Lys, Asp, and Glu) in the N-terminal region (Figures 4C and 5); the C-terminal region, including the disordered tail, contains only one charged side chain, Lys45.

Structural comparison of ι-RXIA[L-Phe44] using Dali (*37*) revealed that there are no other known structures with a Dali *Z*-score larger than 2, over either the whole 46 residues (Table S3 in Supporting Information) or just the well-defined Cys5−Leu35 region. The toxin versutoxin (*16*) (RCSB accession number 1VTX), which contains a triple-stranded antiparallel β-sheet and has the same pattern of disulfide connectivities as ι-RXIA[L-Phe44], is the closest match, with a Dali *Z*-score of 0.6. ω-Agatoxin IVB (*38*), ω-agatoxin IVA (*39*), and ι-RXIA[L-Phe44] contain four disulfide bridges, but in the case of ω-agatoxins IVA and IVB the fourth disulfide is located within one of the loops, whereas in ι-RXIA-[L-Phe44] it connects one of the loops to the C-terminus. It is interesting to note that there are similarities between ι-RXIA and ω-agatoxin IVB (RCSB accession number 1AGG), which has D-Ser at position 46 (*38*, *40*, *41*) (note that in ref *35*, ω-agatoxin IVB is referred to as ω-agatoxin TK) and an unstructured C-terminal region (residues 37−48).

Figure S4 in Supporting Information shows the superposition of ι-RXIA[L-Phe] with ω-agatoxin IVB, robustoxin (RCSB accession number 1QDP), versutoxin (RCSB accession number 1VTX), and J-ACTX-Hv1c (RCSB accession number 1DLO). The pairwise RMSDs between ι-RXIA-[L-Phe] and the above four molecules, superimposed over N, C^α, and C of the β-sheet and C^α and C^β of the three disulfides of the ICK fold, are 2.80, 3.72, 3.39, and 1.32 Å, respectively.

Comparison of ι-RXIA[L-Phe44] with ι-RXIA. Figure 2 shows that ι-RXIA[L-Phe44] and ι-RXIA have a similar pattern of backbone NH and $C^\alpha H$ chemical shift deviations from random coil values at pH 5.9 and 25 °C. The differences in backbone $C^\alpha H$ and NH and side chain $C^\beta H$ chemical shifts between ι-RXIA[L-Phe44] and ι-RXIA (Figure 2C) are very small, the largest being <0.3 ppm. The main differences occur adjacent to Phe44 (residues 38−46), although the NH of Leu35 is perturbed and there are some small changes more distant from Phe44, notably for Cys18 and Ser30. Comparison of 800 MHz NOESY spectra of the two peptides showed that there were very few NOE differences between them (see comparison in Figure S3 in Supporting Information). The same is true for the backbone $^3J_{HNN\alpha}$ coupling constants (Tables S1 and S2 in Supporting Information), although small differences are evident around residue 44.

In order to confirm our inference from comparison of chemical shifts, backbone coupling constants, and NOE distribution that the solution structures of ι-RXIA[L-Phe44] and ι-RXIA were very similar, we have calculated the structure of ι-RXIA using the procedure described above for ι-RXIA[L-Phe44]. The structural statistics for ι-RXIA are compared with those for ι-RXIA[L-Phe44] in Table 1, and the structures are compared in Figure 6. The families of structures are virtually superimposable over the well-defined regions (residues 5−30), as shown in Figure 6 and from RMSD comparisons shown in Figure S5 of the Supporting Information. The N- and C-terminal regions are poorly defined, consistent with the chemical shifts (Figure 2) and lack of medium- and long-range NOEs (Figure S3 in Supporting Information). Thus, even though the regions of conformational space sampled by the families of structures of ι-RXIA and ι-RXIA[L-Phe44] differ slightly in Figure 6, no conclusions can be drawn about the solution conformations of the C-terminal tail containing Phe44 other than that they are disordered in both cases. Comparison of the local structures in the vicinity of Phe44 also reveals no significant differences; the families of structures are similar when superimposed over the backbone heavy atoms of residues 41−45, and the angular averages for the backbone dihedral angles are nearly identical for these residues.

Activity of ι-RXIA on $Na_V1.6$, KCNQ2/3, and $K_V1.2$−1.6 Expressed in Xenopus Oocytes. In previous experiments with frog preparations (*5*, *6*), we observed that ι-RXIA induced repetitive action potentials in motor axons which have $K_V1.2$ (in frogs) and KCNQ2 (and possibly KCNQ3) and $Na_V1.6$ (in mammals) at their nodes of Ranvier as shown by immunohistochemistry (*42*−*44*). The heteromeric human KCNQ (Q2 and Q3) and homomeric human $K_V1.2$, -1.3, -1.4, -1.5, and -1.6 K channels were expressed in *Xenopus* oocytes and tested for their sensitivities to ι-RXIA as described in Experimental Procedures. None of these channels was affected by 100 μM ι-RXIA (not illustrated). In contrast, when ι-RXIA was tested on mouse $Na_V1.6$ expressed in *Xenopus* oocytes, the voltage-gated sodium current (I_{Na}) was affected profoundly. Figure 7 shows representative current traces before (panel A) and after (panel B) ~10 min exposure to 5 μM ι-RXIA. For a given voltage step, the peptide increased the peak I_{Na}. To facilitate comparison, the responses to a −30 mV voltage step in the absence and presence of ι-RXIA are superimposed

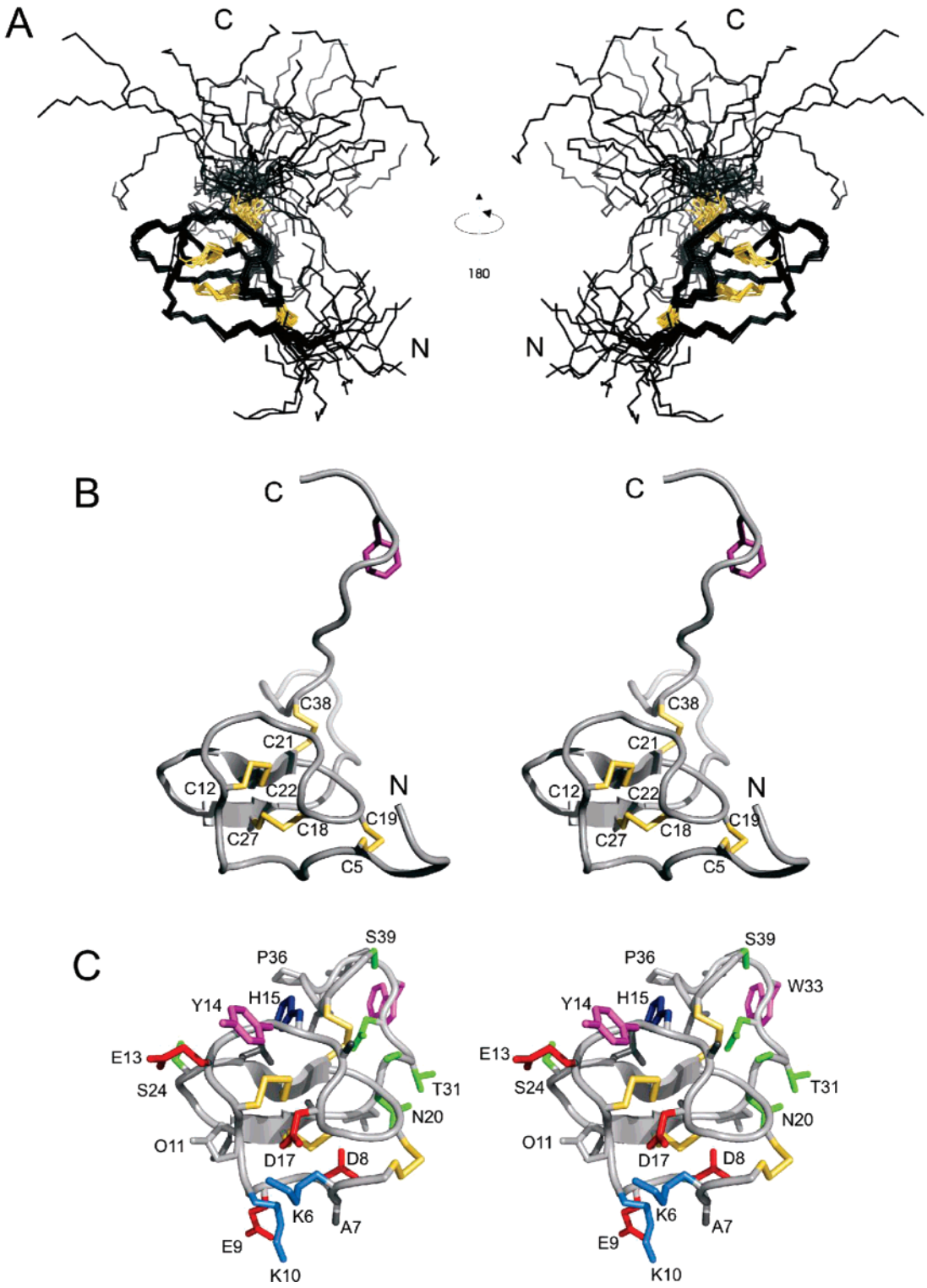

FIGURE 4: Structure of ι-RXIA[L-Phe44]. (A) A family of 20 structures superimposed over backbone heavy atoms of residues 5−30. The disulfide bond connectivities are in yellow. (B) Stereoview of the ribbon diagram of the closest to average structure; the four disulfide bonds (5−19, 12−22, 18−27, 21−38) are in yellow, and Phe44 is in magenta. (C) Stereoview showing only residues 5−39 of the closest to average structure but including all side chains (most of which are labeled with single-letter code and residue number). Side chains are colored as follows: Lys, marine; His, blue; Asp and Glu, red; Trp and Tyr, magenta; Thr, Ser, and Asn, green. This figure was prepared using PyMol.

in Figure 7C. Figure 7D shows that ι-RXIA displaced the voltage dependence of activation to more hyperpolarized potentials ($V_{0.5}$ shifted by 12.5 mV with no significant change in slope factor). In contrast, the toxin affected the voltage dependence of fast inactivation minimally, if at all (Figure 7E). These results indicate that ι-RXIA acted as an agonist of the sodium channel. The effects of ι-RXIA were reversed when the peptide was washed out (not illustrated).

DISCUSSION

The disulfide bond connectivities of ι-RXIA and ι-RXIA-[L-Phe44] have been determined, respectively, by chemical

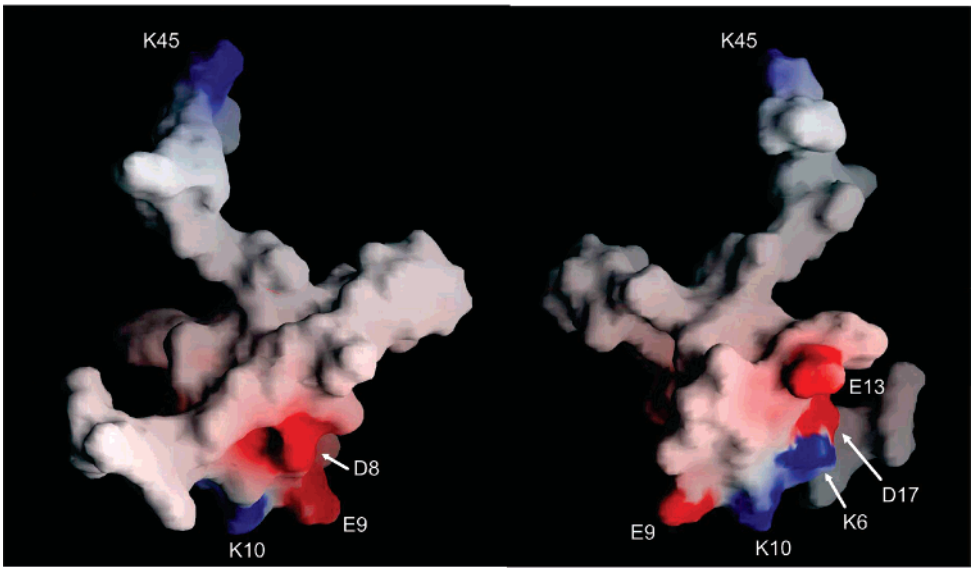

FIGURE 5: Surface representation of the closest to average structure of ι-RXIA[L-Phe44]. The surface is colored, with basic residues in blue and acidic residues in red. The two views are related by a 180° rotation around the vertical axis. This figure was prepared using GRASP (*29*).

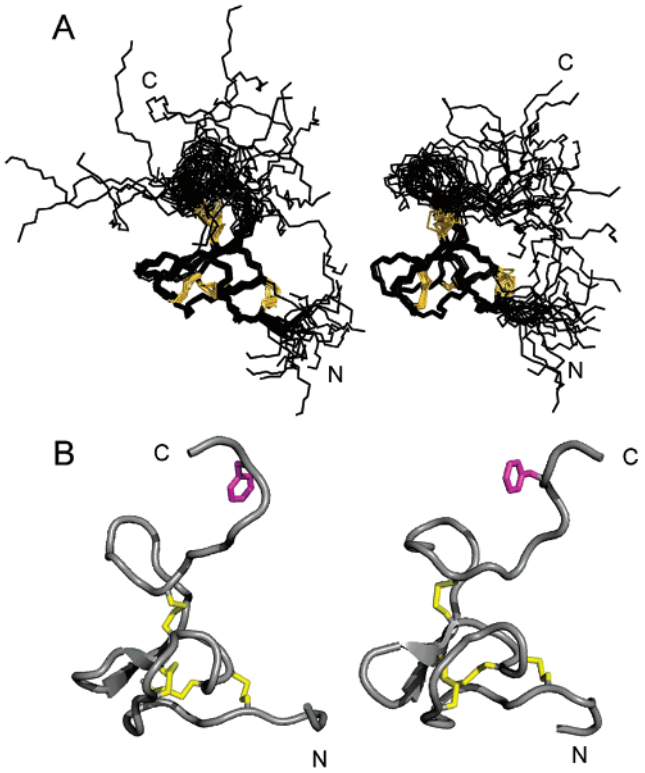

FIGURE 6: Comparison of structures of ι-RXIA and ι-RXIA[L-Phe44]. (A) Families of 20 structures of ι-RXIA (left) and ι-RXIA-[L-Phe44] (right) superimposed over the backbone heavy atoms of residues 5−30 in each case. The disulfide bond connectivities are in orange. (B) Ribbon diagram of the closest to average structures of ι-RXIA (left) and ι-RXIA[L-Phe44] (right); these are the closest to average structures in each case following superposition of each family over the entire backbone (residues 1−46). The four disulfide bonds (5−19, 12−22, 18−27, 21−38) are in yellow, and Phe44 is in magenta.

mapping and analysis of structures calculated using NMR-derived restraints. The solution structure shows that ι-RXIA forms an ICK-fold motif stabilized by the three disulfide bridges Cys5−Cys19, Cys12−Cys22, and Cys18−Cys27, with one additional disulfide (Cys21−Cys38) linking the ICK motif to the C-terminus. This is the same pattern seen in the Sydney funnel web spider toxin, robustoxin, i.e., I−IV/II−VI/III−VII/V−VIII (*15*). However, in a different spider toxin, J-atracotoxin, which shares an identical cysteine framework with I-conotoxins (Figure 1), NMR studies, combined with a partial reduction/alkylation technique, showed that the cysteine connectivities were I−VI, II−VII, III−IV, and V−VIII, as illustrated in Figure 8. An unusual feature of J-atracotoxin is the presence of a rare vicinal disulfide bridge (CysIII−CysIV), which appears to be critical for the insecticidal activity of this polypeptide (*12*). Thus, apparently conserved cysteine frameworks do not lead to the same disulfide connectivities. ι-RXIA is more similar to J-atracotoxin (in terms of spacing between cysteine residues) than to some other I-superfamily members characterized from *Conus*. It remains to be seen what the disulfide linkages are in other framework 11 *Conus* peptides, such as the I_2-superfamily conotoxin BtX (Figure 1).

Robustoxin and versutoxin have the same pattern of disulfide connectivities as ι-RXIA (I−IV/II−VI/III−VII/V−VIII) even though they do not have the -C-C-CC-CC-C-C- pattern characteristic of framework 11. They also adopt ICK motif structures (*15*, *16*), with the fourth disulfide linking this motif to the C-terminus (*15*). Structurally, therefore, they are more similar to ι-RXIA than is J-atracotoxin, even though the latter has a framework 11 arrangement of cysteine residues. A possible reason for this difference is the presence of Pro between the CC doublets in the J-atracotoxins (*12*), in contrast to the Asn present in ι-RXIA (Figure 1A) and related peptides from *C. radiatus* (*5*, *7*), although other conserved non-Cys residues may also have important roles as folding determinants for this disulfide framework. Thus, different patterns of half-cystines but the same disulfide connectitivies (as in ι-RXIA and robustoxin) can produce similar structures, but the same pattern of half-cystines (as in ι-RXIA and J-atracotoxin) does not necessarily lead to the same pattern of disulfide connectitivies (Figure 8). A remarkable feature of all of these molecules, however, is the

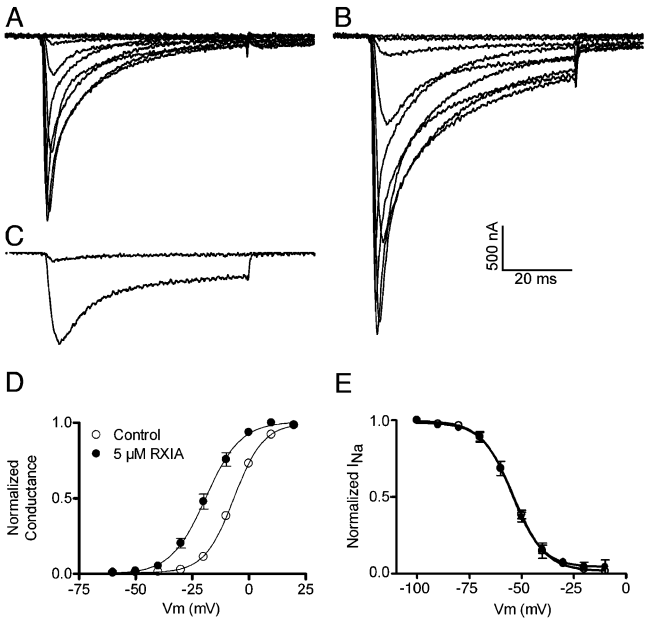

FIGURE 7: ι-RXIA promotes the activation of $Na_V1.6$ without significantly affecting channel inactivation. *Xenopus* oocytes expressing mouse $Na_V1.6$ were prepared and used as described in Experimental Procedures. Oocytes were clamped at −100 mV, and 60 ms depolarizing steps were applied in 10 mV increments from −60 to +20 mV. Representative sodium currents (I_{Na}) in control solution (A) and after the effects of 5 μM ι-RXIA had reached steady-state in about 10 min (B). The peak amplitudes of I_{Na} were increased by the peptide. (C) One trace each from (A) and (B) representing the responses to a −30 mV voltage step are superimposed and illustrate the dramatic effect of ι-RXIA on I_{Na} at this potential. When their peaks were normalized, the traces essentially overlapped (not illustrated), indicating that toxin treatment does not alter the time course of I_{Na}. (D) The voltage dependence of activation was shifted to more hyperpolarized potentials by ι-RXIA. Solid lines represent Boltzmann fits: $V_{0.5}$ values were −6.64 ± 0.27 mV (control) and −19.09 ± 0.74 mV (with peptide); respective slope factors were 6.50 ± 0.24 and 7.72 ± 0.69, which were not significantly different from one another ($p < 0.5$, Student's t-test). (E) Voltage dependence of inactivation was essentially unaltered by 5 μM ι-RXIA. The pulse protocol for inactivation was as described in Experimental Procedures. Solid lines are Boltzmann fits: inactivation $V_{0.5}$ values were −54.02 ± 0.74 mV (control) and −54.49 ± 0.69 mV (with toxin); respective slope factors were 7.60 ± 0.67 and 7.25 ± 0.63. The symbol legend in (D) applies to both (D) and (E), and data points in (D) and (E) represent the mean ± SE ($N = 3$ oocytes).

prevalence of the ICK structural motif (*33*, *34*), or minor variants thereof, as the basic structural scaffold. It is possible that both *Conus* and spider peptides may have arisen from peptides with a disulfide connectivity characteristic of the ICK motif and that the fourth disulfide bond was added subsequently (Figure 8). The identical structural motif of knotted cystines is characteristic of another superfamily of *Conus* peptides, the O-superfamily (*45*, *46*). The I-conotoxins (framework 11) and O-conotoxins (defined by framework 6, C-C-CC-C-C) belong to distinct gene superfamilies, and there is no evident homology between their precursor sequences (*7*, *47*), reflecting a long period of evolutionary divergence.

Comparison of the chemical shifts, backbone coupling constants, and NOEs of ι-RXIA with those of ι-RXIA[L-Phe44] suggests that posttranslational modification of residue 44 from L to D has very little effect on the structure. This is readily accounted for by the structure described in this paper,

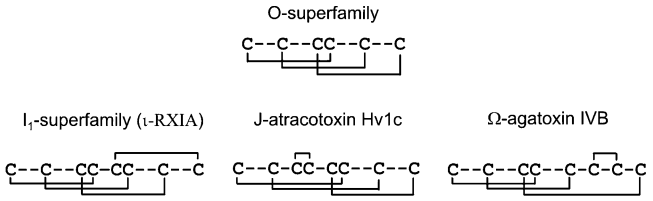

FIGURE 8: Disulfide patterns in toxins containing three and four disulfide bridges. The O-conotoxins (framework 6) have the disulfide pattern I−IV/II−V/III−VI. The I-conotoxins (framework 11), including ι-RXIA, have the disulfide pattern I−IV/II−VI/III−VII/V−VIII, as do robustoxin and versutoxin. The spider toxin, J-atracotoxin, which shares an identical cysteine framework with the I-conotoxins, has the disulfide pattern I−VI/II−VII/III−IV/V−VIII. Yet another pattern of connectivities of eight half-cystines is found in ω-agatoxin IVB. The disulfide bridges above each of the amino acid sequences show the different ways in which the fourth bridge could have been added to the ICK pattern of three bridges in the course of evolution.

as the C-terminal region beyond the last disulfide bridge (Cys21−Cy38) is largely disordered in both structures. As the naturally occurring D-Phe44 form of ι-RXIA is significantly more active as an excitotoxin than the L-Phe44 analogue both in vitro and in vivo (*6*), it is likely that the C-terminal tail of ι-RXIA undergoes a transition to a more ordered conformation when in complex with its receptor. In this conformation the switch from D to L configuration at Phe44 may be expected to have a significant effect on affinity and/or activity. The more structured region of ι-RXIA, the ICK motif, probably plays a common role in both ι-RXIA and ι-RXIA[L-Phe44] of mediating peptide binding to the appropriate site on the target in such a way as to allow the C-terminal tail to interact with neighboring residues.

The functional importance of epimerization of a single amino acid near the C-terminus was also observed for ω-agatoxin IVB, which has a similar combination of an ICK motif core and an unstructured tail (*13*, *38*, *40*, *41*). In this 48-residue peptide, D-Ser46 was crucial for the inhibition of P-type calcium channels, whereas the L-Ser enantiomer was about 90-fold less active (*40*).

As with the funnel web spider toxins robustoxin and versutoxin, with which it shares a common disulfide pattern and structures, ι-RXIA proves to be active against sodium channels. The agonistic action of ι-RXIA on $Na_V1.6$ (Figure 7) explains how the peptide renders motor axons hyperexcitable, as it effectively lowers the threshold for the generation of action potentials by shifting the voltage sensitivity of the sodium channels. The effect of ι-RXIA in shifting the voltage dependence of activation in a hyperpolarizing direction is reminiscent of δ-conopeptides PVIA and SVIE (*48*). However, unlike the δ-conopeptides, ι-RXIA does not shift the voltage dependence of steady-state inactivation appreciably, if at all (Figure 7E). Further experiments are in progress to examine ι-RXIA's VGSC subtype selectivity as well as its mechanism of action in greater detail. However, it is noteworthy that there is a convergence of structure and function in ι-RXIA, as its structure resembles those of funnel web spider toxins that also target sodium channels. Their effects on these channels, however, are not identical, and it will be of interest to define which residues in ι-RXIA differentiate its activity on the sodium channel from those of robustoxin and versutoxin and what the respective roles

of the ICK core and the C-terminal tail containing Phe44 are in their activities.

ACKNOWLEDGMENT

We thank Shenggen Yao for help with the NMR experiments, Zhi-Ping Feng and Jennifer Sabo for help with the structure calculations, Alan Goldin for the mouse $Na_V1.6$ clone, Layla Azam for preparing the corresponding cRNA, Michael Sanguinetti for help with testing KCNQ clones, and Minmin Zhang for helpful discussions.

SUPPORTING INFORMATION AVAILABLE

NMR data and structure comparisons referred to in the text. This material is available free of charge via the Internet at http://pubs.acs.org.

REFERENCES

1. Terlau, H., and Olivera, B. M. (2004) *Conus* venoms: a rich source of novel ion channel-targeted peptides, *Physiol. Rev. 84*, 41−68.
2. Norton, R. S., and Olivera, B. M. (2006) Conotoxins down under, *Toxicon 48*, 780−798.
3. Olivera, B. M. (2006) *Conus* peptides: biodiversity-based discovery and exogenomics, *J. Biol. Chem. 281*, 31173−31177.
4. Buczek, O., Bulaj, G., and Olivera, B. M. (2005) Conotoxins and the posttranslational modification of secreted gene products, *Cell Mol. Life Sci. 62*, 3067−3079.
5. Jimenez, E. C., Shetty, R. P., Lirazan, M., Rivier, J., Walker, C., Abogadie, F. C., Yoshikami, D., Cruz, L. J., and Olivera, B. M. (2003) Novel excitatory *Conus* peptides define a new conotoxin superfamily, *J. Neurochem. 85*, 610−621.
6. Buczek, O., Yoshikami, D., Bulaj, G., Jimenez, E. C., and Olivera, B. M. (2005) Post-translational amino acid isomerization: a functionally important D-amino acid in an excitatory peptide, *J. Biol. Chem. 280*, 4247−4253.
7. Buczek, O., Yoshikami, D., Watkins, M., Bulaj, G., Jimenez, E. C., and Olivera, B. M. (2005) Characterization of D-amino-acid-containing excitatory conotoxins and redefinition of the I-conotoxin superfamily, *FEBS J. 272*, 4178−4188.
8. Kauferstein, S., Huys, I., Kuch, U., Melaun, C., Tytgat, J., and Mebs, D. (2004) Novel conopeptides of the I-superfamily occur in several clades of cone snails, *Toxicon 44*, 539−548.
9. Fan, C. X., Chen, X. K., Zhang, C., Wang, L. X., Duan, K. L., He, L. L., Cao, Y., Liu, S. Y., Zhong, M. N., Ulens, C., Tytgat, J., Chen, J. S., Chi, C. W., and Zhou, Z. (2003) A novel conotoxin from *Conus betulinus*, κ-BtX, unique in cysteine pattern and in function as a specific BK channel modulator, *J. Biol. Chem. 278*, 12624−12633.
10. Kauferstein, S., Huys, I., Lamthanh, H., Stocklin, R., Sotto, F., Menez, A., Tytgat, J., and Mebs, D. (2003) A novel conotoxin inhibiting vertebrate voltage-sensitive potassium channels, *Toxicon 42*, 43−52.
11. Olivera, B. M., and Cruz, L. J. (2001) Conotoxins, in retrospect, *Toxicon 39*, 7−14.
12. Wang, X., Connor, M., Smith, R., Maciejewski, M. W., Howden, M. E., Nicholson, G. M., Christie, M. J., and King, G. F. (2000) Discovery and characterization of a family of insecticidal neurotoxins with a rare vicinal disulfide bridge, *Nat. Struct. Biol. 7*, 505−513.
13. Adams, M. E., Mintz, I. M., Reily, M. D., Thanabal, V., and Bean, B. P. (1993) Structure and properties of ω-agatoxin IVB, a new antagonist of P-type calcium channels, *Mol. Pharmacol. 44*, 681−688.
14. Maggio, F., and King, G. F. (2002) Scanning mutagenesis of a Janus-faced atracotoxin reveals a bipartite surface patch that is essential for neurotoxic function, *J. Biol. Chem. 277*, 22806−22813.
15. Pallaghy, P. K., Alewood, D., Alewood, P. F., and Norton, R. S. (1997) Solution structure of robustoxin, the lethal neurotoxin from the funnel-web spider *Atrax robustus*, *FEBS Lett. 419*, 191−196.
16. Fletcher, J. I., Chapman, B. E., Mackay, J. P., Howden, M. E., and King, G. F. (1997) The structure of versutoxin (δ-atracotoxin-Hv1) provides insights into the binding of site 3 neurotoxins to the voltage-gated sodium channel, *Structure 5*, 1525−1535.
17. Gray, W. R. (1993) Disulfide structures of highly bridged peptides: a new strategy for analysis, *Protein Sci. 2*, 1732−1748.
18. Gibbs, S. J., and Johnson, C. S. (1991) A PFG-NMR experiment for accurate diffusion and flow studies in the presence of eddy currents, *J. Magn. Reson. 93*, 395−402.
19. Dingley, A. J., Mackay, J. P., Chapman, B. E., Morris, M. B., Kuchel, P. W., Hambly, B. D., and King, G. F. (1995) Measuring protein self-association using pulsed-field-gradient NMR spectroscopy: application to myosin light chain 2, *J. Biomol. NMR 6*, 321−328.
20. Yao, S., Howlett, G. J., and Norton, R. S. (2000) Peptide self-association in aqueous trifluoroethanol monitored by pulsed field gradient NMR diffusion measurements, *J. Biomol. NMR 16*, 109−119.
21. Bartels, C., Xia, T.-H., Billeter, M., Güntert, P and Wüthrich, K. (1995) The program XEASY for computer-supported NMR spectral analysis of biological macromolecules, *J. Biomol. NMR 6*, 1−10.
22. Palmer, A. G., Cavanagh, J., Wright, P. E., and Rance, M. (1991) Sensitivity improvement in proton-detected two-dimensional heteronuclear correlation NMR spectroscopy, *J. Magn. Reson. 93*, 151−170.
23. Kay, L. E., Keifer, P., and Saarinen, T. (1992) Pure absorption gradient enhanced heteronuclear single quantum correlation spectroscopy with improved sensitivity, *J. Am. Chem. Soc. 114*, 10663−10665.
24. Herrmann, T., Güntert, P., and Wüthrich, K. (2002) Protein NMR structure determination with automated NOE assignment using the new software CANDID and the torsion angle dynamics algorithm DYANA, *J. Mol. Biol. 319*, 209−227.
25. Schwieters, C. D., Kuszewski, J. J., Tjandra, N., and Clore, G. M. (2003) The XPLOR-NIH NMR molecular structure determination package, *J. Magn. Reson. 160*, 65−73.
26. Laskowski, R. A., Rullmannn, J. A., MacArthur, M. W., Kaptein, R., and Thornton, J. M. (1996) AQUA and PROCHECK-NMR: programs for checking the quality of protein structures solved by NMR, *J. Biomol. NMR 8*, 477−486.
27. Koradi, R., Billeter, M., and Wüthrich, K. (1996) MOLMOL: a program for display and analysis of macromolecular structures, *J. Mol. Graphics 14*, 29−32.
28. DeLano, W. L. (2002) The PyMol Molecular Graphics System, DeLano Scientific, San Carlos, CA (http://www.pymol.org).
29. Nicholls, A., Sharp, K. A., and Honig, B. (1991) Protein folding and association: insights from the interfacial and thermodynamic properties of hydrocarbons, *Proteins 11*, 281−296.
30. Seavey, B. R., Farr, E. A., Westler, W. M., and Markley, J. L. (1991) A relational database for sequence-specific protein NMR data, *J. Biomol. NMR 1*, 217−236.
31. Wishart, D. S., Bigam, C. G., Holm, A., Hodges, R. S., and Sykes, B. D. (1995) ^{1}H, ^{13}C and ^{15}N random coil NMR chemical shifts of the common amino acids. I. Investigations of nearest-neighbor effects, *J. Biomol. NMR 5*, 67−81.
32. Corzo, G., Sabo, J. K., Bosmans, F., Billen, B., Villegas, E., Tytgat, J., and Norton, R. S. (2007) Solution structure and alanine scan of a spider toxin that affects the activation of mammalian voltage-gated sodium channels, *J. Biol. Chem. 282*, 4643−4652.
33. Pallaghy, P. K., Nielsen, K. J., Craik, D. J., and Norton, R. S. (1994) A common structural motif incorporating a cystine knot and a triple-stranded β-sheet in toxic and inhibitory polypeptides, *Protein Sci. 3*, 1833−1839.
34. Norton, R. S., and Pallaghy, P. K. (1998) The cystine knot structure of ion channel toxins and related polypeptides, *Toxicon 36*, 1573−1583.
35. Miles, L. A., Dy, C. Y., Nielsen, J., Barnham, K. J., Hinds, M. G., Olivera, B. M., Bulaj, G., and Norton, R. S. (2002) Structure of a novel P-superfamily spasmodic conotoxin reveals an inhibitory cystine knot motif, *J. Biol. Chem. 277*, 43033−43040.
36. Berman, H. M., Westbrook, J., Feng, Z., Gilliland, G., Bhat, T. N., Weissig, H., Shindyalov, I. N., and Bourne, P. E. (2000) The Protein Data Bank, *Nucleic Acids Res. 28*, 235−242.
37. Holm, L., and Sander, C. (1998) Touring protein fold space with Dali/FSSP, *Nucleic Acids Res. 26*, 316−319.
38. Yu, H., Rosen, M. K., Saccomano, N. A., Phillips, D., Volkmann, R. A., and Schreiber, S. L. (1993) Sequential assignment and structure determination of spider toxin ω-Aga-IVB, *Biochemistry 32*, 13123−13129.
39. Kim, J. I., Konishi, S., Iwai, H., Kohno, T., Gouda, H., Shimada, I., Sato, K., and Arata, Y. (1995) Three-dimensional solution structure of the calcium channel antagonist ω-agatoxin IVA:

consensus molecular folding of calcium channel blockers, *J. Mol. Biol. 250*, 659−671.
40. Kuwada, M., Teramoto, T., Kumagaye, K. Y., Nakajima, K., Watanabe, T., Kawai, T., Kawakami, Y., Niidome, T., Sawada, K., Nishizawa, Y., et al. (1994) ω-agatoxin-TK containing D-serine at position 46, but not synthetic ω-[L-Ser46]agatoxin-TK, exerts blockade of P-type calcium channels in cerebellar Purkinje neurons, *Mol. Pharmacol. 46*, 587−593.
41. Reily, M. D., Thanabal, V., and Adams, M. E. (1995) The solution structure of ω-Aga-IVB, a P-type calcium channel antagonist from venom of the funnel web spider, *Agelenopsis aperta*, *J. Biomol. NMR 5*, 122−132.
42. Caldwell, J. H., Schaller, K. L., Lasher, R. S., Peles, E., and Levinson, S. R. (2000) Sodium channel $Na_V1.6$ is localized at nodes of Ranvier, dendrites, and synapses, *Proc. Natl. Acad. Sci. U.S.A. 97*, 5616−5620.
43. Rasband, M. N. (2004) It's "juxta" potassium channel!, *J. Neurosci. Res. 76*, 749−757.
44. Schwarz, J. R., Glassmeier, G., Cooper, E. C., Kao, T. C., Nodera, H., Tabuena, D., Kaji, R., and Bostock, H. (2006) KCNQ channels mediate IKs, a slow K^+ current regulating excitability in the rat node of Ranvier, *J. Physiol. 573*, 17−34.
45. McIntosh, J. M., Hasson, A., Spira, M. E., Gray, W. R., Li, W., Marsh, M., Hillyard, D. R., and Olivera, B. M. (1995) A new family of conotoxins that blocks voltage-gated sodium channels, *J. Biol. Chem. 270*, 16796−16802.
46. Shon, K. J., Stocker, M., Terlau, H., Stuhmer, W., Jacobsen, R., Walker, C., Grilley, M., Watkins, M., Hillyard, D. R., Gray, W. R., and Olivera, B. M. (1998) κ-Conotoxin PVIIA is a peptide inhibiting the shaker K^+ channel, *J. Biol. Chem. 273*, 33−38.
47. Kauferstein, S., Melaun, C., and Mebs, D. (2005) Direct cDNA cloning of novel conopeptide precursors of the O-superfamily, *Peptides 26*, 361−367.
48. West, P. J., Bulaj, G., and Yoshikami, D. (2005) Effects of δ-conotoxins PVIA and SVIE on sodium channels in the amphibian sympathetic nervous system, *J. Neurophysiol. 94*, 3916−3924.

BI700797F